Int. J. Solids Structures, 1977, Vol. 13, pp. 561–570. Pergamon Press. Printed in Great Britain

THE ROLE OF THE ADHESIVE LAYER IN A DOUBLE CANTILEVER JOINT

F. FARHAD
Gruen Associates, Los Angeles, CA 90048, U.S.A.

and

R. MUKI and R. A. WESTMANN
Mechanics and Structures Department, School of Engineering and Applied Science, University of California, Los Angeles, CA 90024, U.S.A.

(*Received* 12 *July* 1976; *revised* 1 *November* 1976)

Abstract—The problem of a double cantilever beam adhesive joint is reconsidered under the assumption of cohesive fracture within the adhesive bond layer. After properly accounting for the adhesive layer, the problem is reduced to a Fredholm integral equation of the second kind for the bond line traction. Numerical results for the bond line stress distribution and the crack tip stress intensity factor are presented for several combinations of the governing material and geometrical parameters.

1. INTRODUCTION

In one of the first fracture studies in adhesive mechanics, Mostovoy and Patrick[1] successfully measured the strain energy release rate $\mathcal{G}_c$. Using a tapered double cantilever beam for their adhesive-adherend system they measured the energy required to create new surface for a cohesive crack propagating in the adhesive layer in opening mode.

In conducting analytical or numerical stress analyses of adhesive joints it is common to neglect the role or presence of the bonding layer. Justification for this is usually based on the "thinness" of the adhesive as compared to the local adherend thickness. While such results are useful in indicating loading and geometry effects, the resulting crack tip stress intensity factors can be quite misleading. The actual fracture takes place by the separation of adhesive material (cohesive failure) and so it is necessary to determine the stress intensity factor accounting for the local effects in the neighborhood of the crack.

Of course if one calculates or experimentally measures the strain energy release rate for an adhesive-adherend system and then determines $\mathcal{G}_c$ the answer is correct. However, this result is only valid for that particular adhesive-adherend combination. Should the same adhesive be used with a different adherend material the joint properties would have to be re-evaluated. Thus, the knowledge of the strain energy release rate of an adhesive-adherend system supplies no information about the fracture properties of the adhesive itself.

It is desirable to know the fracture properties of the adhesive alone as they will characterize the strength of the joint for all possible selections of adherend materials. To complete such a characterization one requires knowledge of the crack tip stress intensity factors within the adhesive layer where the role of the layer thickness and mechanical properties of the adhesive have been properly accounted for. It is a purpose of this paper to present the results of such an analysis for a double cantilever adhesive joint.

Theoretical analysis and numerical results have been presented in [2] for a double cantilever beam disregarding the presence of the adhesive layer. The analysis presented herein is similar to that employed in [2] except for the incorporation of the bonding layer as a two dimensional elastic continuum and the use of a two variable expansion procedure to expedite evaluation of certain integrals.

The effects of the ratio of Young's modulus of adherend to that of adhesive and of the adhesive thickness to that of adherend on bond stress distribution and stress intensity factor are presented graphically. It is found that the influence of the ratio of Young's moduli is more pronounced than that of the thickness ratio. Numerical results indicate that joint strength improves with the increase of adherend Young's modulus and with the decrease of adherend thickness. These results are in agreement with previous experimental observation[3]. It is

observed that the stress intensity factor increases linearly with l (the distance from the crack edge to the point of load application) if l is larger than $3h$, h being the adherend thickness. We therefore introduce a dimensionless asymptotic approximation for the stress intensity factor as a linear function of l/h. The constants in this linear form depend only on the thickness ratio and upon the ratio of Young's moduli if the bond length is larger than $3h$. These constants are presented graphically for a wide range of these ratios.

2. FORMULATION OF THE PROBLEM. REDUCTION TO A FREDHOLM INTEGRAL EQUATION

The actual problem to be modeled, Fig. 1(a), consists of two adherends bonded together along a finite line segment by a thin layer of adhesive material. The connection is loaded by a pair of equal and opposite loads tending to separate or cleave the connection along the adhesive line. We wish to calculate the stress distribution in the adhesive layer in order to estimate the maximum load P that may be applied to the adhesive joint.

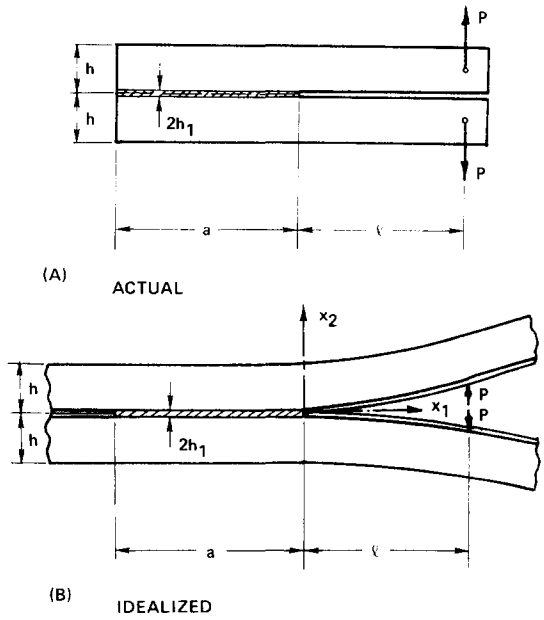

Fig. 1. The actual and idealized configurations of the double cantilever beam.

To facilitate the analysis, let the upper and lower adherends be infinite in extent, each having a plate thickness $h - h_1$. The adhesive layer is also taken to be infinite in extent having a uniform thickness $2h_1$. Both adherends and adhesive layer are assumed to be composed of isotropic, homogeneous and linearly elastic materials with Young's modulus E_γ and Poisson's ratio ν_γ ($\gamma = 1, 2$) where subscripts 1, 2 are for the adhesive and adherends respectively.

As shown in Fig. 1(b), the adhesive layer is perfectly bonded to the two adherends while the midplane of the adhesive layer is separated by a traction free crack except for a connection distance a.

A rectangular cartesian coordinate system is introduced with the x_1, x_3 plane lying in the middle of adhesive layer and in such a way that the connection corresponds to the region $-a < x_1 < 0, -\infty < x_3 < \infty$. The loading consists of two concentrated line loads applied to the faces of the cracked adhesive surface at points $x_1 = l$ and $x_2 = 0\pm$.

Because of the symmetry of the problem, we need only to consider the stress and displacement fields in the upper half ($x_2 \geq 0$) of the joint. The solution for the stress and displacement fields is to be obtained within the scope of two dimensional classical elastostatics for a state of plane strain.

Denote the displacements and stresses in the upper half of the adhesive layer by $u_\alpha^{(1)}$, $\tau_{\alpha\beta}^{(1)}$, while $u_\alpha^{(2)}$ and $\tau_{\alpha\beta}^{(2)}$ are those in the upper adherend ($\alpha, \beta = 1, 2$). Then the boundary and bond conditions become

$$\tau_{\alpha 2}^{(2)}(x_1, h) = 0, \quad \tau_{12}^{(1)}(x_1, 0) = 0 \quad (-\infty < x_1 < \infty), \tag{1a}$$

$$\tau_{22}^{(1)}(x_1, 0) = -P\delta(x_1 - l) \quad (-\infty < x_1 < -a,\ 0 < x_1 < \infty), \tag{1b}$$

$$u_{2,1}^{(1)}(x_1, 0) = \omega \quad (-a < x_1 < 0), \tag{1c}$$

where δ is the Dirac delta function and ω is the slope of the bond line relative to that of the edge as $x \to \infty$. The continuity conditions at $x_2 = h_1$ are

$$\left.\begin{aligned} \tau_{\alpha 2}^{(1)}(x_1, h_1) &= \tau_{\alpha 2}^{(2)}(x_1, h_1), \\ u_{\alpha,1}^{(1)}(x_1, h_1) &= u_{\alpha,1}^{(2)}(x_1, h_1) \quad (-\infty < x_1 < \infty). \end{aligned}\right\} \tag{2}$$

To these conditions we have to add the regularity requirements

$$\tau_{\alpha\beta}^{(\gamma)}(x_1, x_2) = o(1) \quad \text{as } |x_1| \to \infty \ (\gamma = 1, 2). \tag{3}$$

The only unknown stress on the boundary of the upper half of the adhesive joint is

$$\tau_{22}^{(1)}(x_1, 0) = p(x) \quad (-a < x_1 < 0). \tag{4}$$

In view of the overall equilibrium requirements for the upper half of the joint $p(x)$ must satisfy the constraint conditions:

$$\int_{-a}^{0} p(x)\,dx - P = 0, \quad \int_{-a}^{0} xp(x)\,dx - lP = 0. \tag{5}$$

To expedite the derivation of the solution to the problem just formulated we introduce a singular field (Green's function) with displacement $\mathring{u}_\alpha$ and stress $\mathring{\tau}_{\alpha\beta}$. This singular field is the solution to the elastostatic problem characterized by the boundary conditions (1a,b) with P, l, a replaced by 1, 0, 0, and the continuity conditions (2). In addition the following regularity requirements must be enforced:

$$\left.\begin{aligned} \mathring{\tau}_{\alpha\beta}^{(\gamma)}(x_1, x_2) &= 0(e^{-cx_1}) \qquad \text{as } x_1 \to \infty, \\ \mathring{\tau}_{\alpha\beta}^{(\gamma)}(x_1, x_2) &= 0(|x|^k) \qquad \text{as } x_1 \to -\infty \ (\gamma = 1, 2) \end{aligned}\right\} \tag{6}$$

where c and k are positive constants.

In contrast to the original problem, this singular solution is obtained by the routine application of exponential Fourier transforms and yields real integral representations for $\mathring{u}_\alpha$ and $\mathring{\tau}_{\alpha\beta}$.

A key item in the formulation of the main problem is $\mathring{u}_{2,1}^{(1)}$ along the lower edge. This quantity is determined to be

$$\mathring{u}_{2,1}^{(1)}(x_1, 0) = -\frac{2(1-\nu_1^2)}{\pi h E_1}\left[\frac{h}{x_1} + F\left(\frac{x_1}{h}\right)\right] \quad (-\infty < x_1 < \infty), \tag{7}$$

where

$$\left.\begin{aligned} F(\xi) &= -c_1\xi + c_2\xi^3 - F_*(\xi), \\ c_1 &= \frac{3\pi k}{2}\left\{\frac{2}{5} - 2\epsilon\left[\frac{1}{1-\nu_1} - \frac{k}{1-\nu_2} + \frac{6}{5}(k-1)\right]\right\}, \\ c_2 &= \frac{3\pi k}{2}[1 - 3(k-1)\epsilon], \\ F_*(\xi) &= \int_0^\infty \left\{(A_1(s) - 1)\sin(\xi s) - \frac{6k\xi}{s^2}[1 - 3(k-1)\epsilon]\right\} ds \end{aligned}\right\} \tag{8}$$

and

$$\epsilon = \frac{h_1}{h}, \quad k = \frac{E_1(1-\nu_2^2)}{E_2(1-\nu_1^2)}. \tag{9}$$

At this point we recall that the entire dependence of the stress field on the material constants for the type of composite material considered herein can be expressed[2] in terms of two composite parameters, α_* and β_*

$$\alpha_* = \frac{k_*(1-\nu_2)-(1-\nu_1)}{k_*(1-\nu_2)+(1-\nu_1)}, \quad \beta_* = \frac{k_*(1-2\nu_2)-(1-2\nu_1)}{2k_*(1-\nu_2)+2(1-\nu_1)}, \tag{10}$$

where

$$k_* = \frac{\mu_1}{\mu_2} = \frac{1+\nu_2}{1+\nu_1} \cdot \frac{E_1}{E_2}.$$

In fact, the constants c_1 and k in (8) can be written as

$$c_1 = 3\pi k \cdot \left\{\frac{1}{5} - 2\epsilon\left[\frac{\alpha_* - \beta_*}{\alpha_* - 1} + \frac{3}{5}(k-1)\right]\right\}, \tag{11}$$

$$k = \frac{1+\alpha_*}{1-\alpha_*}.$$

The function $A_1(s)$ that appears in the last of (8) results from the solution of four algebraic equations arising from the interface conditions. Expressions for $A_1(s)$ suitable for efficient numerical evaluation for small, intermediate and the large values of s are presented in the Appendix together with a brief explanation of their derivation. These expressions depend on material constants through the parameters α^* and β^* in (10).

If $p(x)$ is known, displacements gradients and stresses in the joint can be evaluated through the use of superposition as follows

$$\left.\begin{aligned} u_{\alpha,1}^{(\gamma)}(x_1, x_2) &= P\mathring{u}_{\alpha,1}^{(\gamma)}(x_1 - l, x_2) - \int_{-a}^{0} p(s)\mathring{u}_{\alpha,1}^{(\gamma)}(x_1 - s, x_2)\,\mathrm{d}s, \\ \tau_{\alpha\beta}^{(\gamma)}(x_1, x_2) &= P\mathring{\tau}_{\alpha\beta}^{(\gamma)}(x_1 - l, x_2) - \int_{-a}^{0} p(s)\mathring{\tau}_{\alpha\beta}^{(\gamma)}(x_1 - s, x_2)\,\mathrm{d}s. \end{aligned}\right\} \quad (\gamma = 1, 2) \tag{12}$$

Now note that the bond condition, the last of (1), yields a singular integral equation for $p(x)$ by use of the first of (12). This singular equation, in turn, is reduced to a regular Fredholm integral equation upon employing Muskhelishvili's technique. The two unknown constants appearing in this process are determined upon enforcing the equilibrium conditions (5). Since the procedure is exactly the same as that employed in [2], we record here only the resulting Fredholm integral equation for the normalized bond traction N.

$$N(\xi) - \int_0^{\alpha} K(\xi, \eta)N(\eta)\,\mathrm{d}\eta = R(\xi) \quad (0 \le \xi \le \alpha) \tag{13}$$

where

$$\left.\begin{aligned} &\xi = -x_1/h, \quad N(\xi) = h\sqrt{\xi(\alpha - \xi)}\,p(-h\xi)/P, \\ \text{and} \\ &\alpha = a/h. \end{aligned}\right\} \tag{14}$$

The Kernel K and the function R are

$$\begin{aligned} K(\xi, \eta) &= \frac{1}{\pi^2\sqrt{\eta(\alpha - \eta)}} \int_0^{\alpha} \sqrt{\zeta(\alpha - \zeta)}\left[\frac{1}{\xi - \zeta} + \frac{4}{\alpha} - \frac{8\xi}{\alpha^2}\right][c_1 - c_2(\zeta - \eta)^2 + F_*(\zeta - \eta)]\,\mathrm{d}\zeta, \\ R(\xi) &= \frac{1}{\pi}\left[\frac{4\lambda}{\alpha} + 3 - \frac{4(\alpha + 2\lambda)}{\alpha}\xi\right] - \frac{1}{\pi^2}\int_0^{\alpha} \sqrt{\zeta(\alpha - \zeta)}\left[\frac{1}{\xi - \zeta} + \frac{4}{\alpha} - \frac{8\xi}{\alpha^2}\right] \\ &\quad \times \left[\frac{1}{\zeta + \lambda} + c_1 - c_2(\lambda + \zeta)^2 + F_*(\lambda + \zeta)\right]\mathrm{d}\zeta \end{aligned} \tag{15}$$

where the constants c_1, c_2 and the function F_* are given by (8) and

$$\lambda = l/h. \tag{16}$$

As apparent from (4) and (12), the stress intensity factor K_I at the loaded end is related to $N(0)$ by

$$K_I = \lim_{x \to 0-} \sqrt{-2\pi x_1}\tau_{22}(x_1, 0) = P\sqrt{\frac{2\pi}{a}}N(0). \tag{17}$$

The numerical determination of the solution to the integral eqn (13) necessitates the evaluation of the infinite integral $F_*(\xi)$ defined by (8). The evaluation of this quantity is greatly expedited by the use of three expressions for $A_1(s)$ in the Appendix for small, intermediate and large values of the argument. The integral equation is reduced to a system of algebraic equations for the values of $N(\xi)$ at a discrete number of mesh points. This reduction is achieved by introducing a partition on the interval $(0, \alpha)$ which is relatively dense near the endpoints where N is expected to vary sharply. The integral in (13) is evaluated by accounting for the square root singularity exactly in the first and last intervals and using the trapezoidal rule over the remainder of the region. Requiring that (13) be satisfied at each of the mesh points then leads to a system of linear algebraic equations for $N(\xi)$.

3. NUMERICAL RESULTS AND DISCUSSION

We proceed now to the discussion of illustrative numerical examples. Figures 2 and 3 depict the variation of the normalized bond stress

$$N(-x_1/h) = \sqrt{-x_1(x_1 + a)}\tau_{22}^{(1)}(x_1, 0)/P \tag{18}$$

along the line of crack propagation. Because of the physical importance of the values of N in the neighborhood of end of the bond line, the stress distributions near the point $x_1/h = 0$ are presented on a magnified scale. In Fig. 2, N is plotted for various ratios of Young's modulus of adherend to that of adhesive, while N is presented in Fig. 3 for several ratios of adherend thickness to adhesive thickness. In both figures, the length of the bonded region, the point of load application and Poisson's ratio are $a/h = 4$, $l/h = 1$ and $\nu_1 = \nu_2 = 0.25$. In Fig. 2, the thickness ratio is $h_1/h = 0.01$ while moduli ratios employed are 2, 10, 20 and 60. These latter values approximately correspond to adherends of wood, glass, aluminum and steel, respectively, if the adhesive is an epoxy resin (Young's modulus 500 ksi (3447 MPa)). Observe in Fig. 2 that both the maximum values and values at $x_1 = 0$ of the normalized bond stress decrease as the ratio of elastic moduli increases. This observation confirms our intuitive feeling that a stiffer adherend leads to a stronger joint for the same adhesive assuming the geometry and the loading pattern are fixed. In Fig. 3 the values of 0.01, 0.02, 0.05 and 0.1 are used for the thickness ratio. It is interesting to note that the thickness ratio has little effect upon the tip value of the normalized

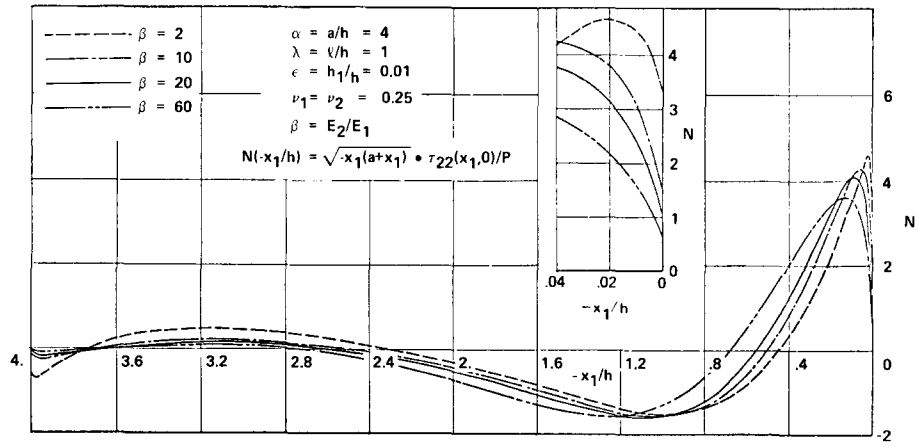

Fig. 2. Distribution of normalized bond stress for various values of β.

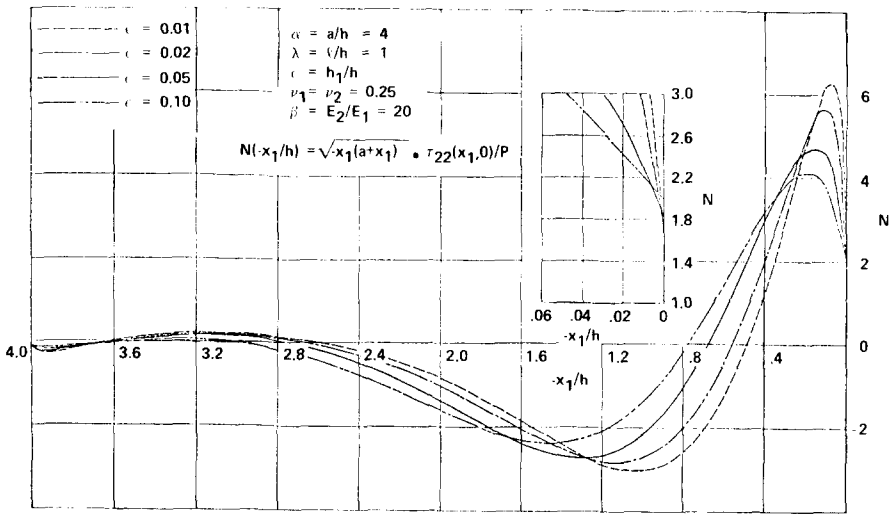

Fig. 3. Distribution of normalized bond stress for various values of ϵ.

bond stress, while the values of N at other points exhibit a greater dependence upon this parameter.

An elementary strength-of-material's type argument suggests that the ratio of the stiffness of the adherend to that of the adhesive might be the only parameter affecting the bond stress distribution. This ratio $[E_2/(h-h_1)]/[E_1/h_1]$ may be approximated closely by $(E_2/E_1)(h_1/h)$ since h_1/h is very small. Figure 4 displays the normalized bond stress distribution for three different combinations of $\beta = E_2/E_1$ and $\epsilon = h_1/h$ all corresponding to a $(E_2/h)/E_1/h_1)$ value of 40, i.e. the same stiffness ratio. These three curves almost coalesce except near the loaded end where, the values differ substantially.

We turn our attention to the singular stress field at the loaded end and introduce a dimensionless stress intensity factor† κ.

$$\kappa(\alpha, \lambda, \epsilon, \beta) = \frac{K_I}{P_0}\sqrt{\frac{h}{2\pi}} = \frac{1}{\sqrt{\alpha}}N(0) \tag{19}$$

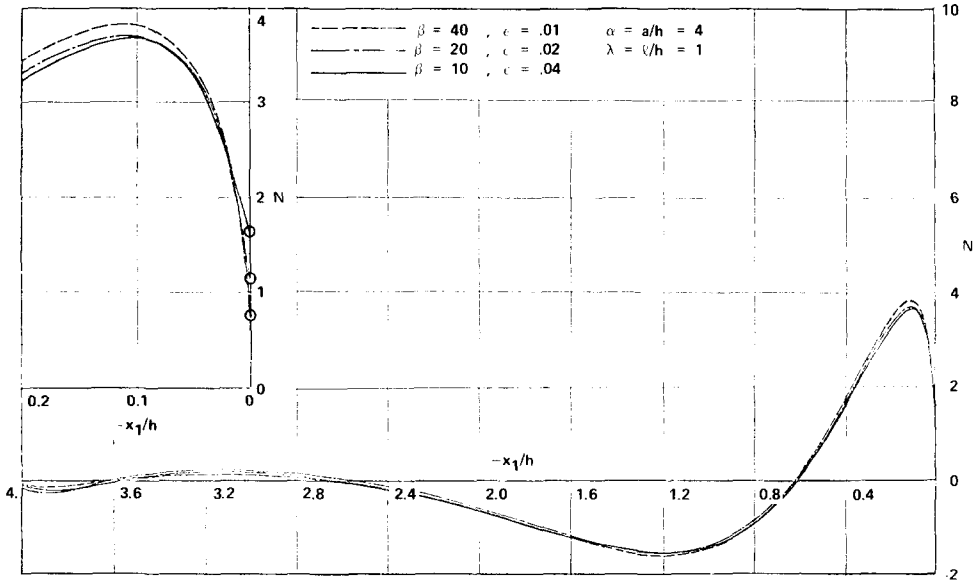

Fig. 4. Distribution of normalized bond stress for various values of ϵ and β such that $\alpha\beta = 0.4$.

†Note that the standard mode 1 stress intensity factor is denoted by K_I.

where the arguments $\alpha = a/h$, $\lambda = l/h$, $\epsilon = h_1/h$ and $\beta = E_2/E_1$ are explicitly written in order to emphasize the dependence upon these parameters.

We observe from Figs. 2 and 3 and similar results not presented here that $N(-x_1/h)$ is very small for $x_1/h < -2.5$ indicating that the interval $-\alpha < x_1/h < -2.5$ does not contribute significantly to the load transfer between the two adherends. This observation indicates that values of α beyond 4, say, will not seriously affect the value $N(0)$. A previous investigation[2] dealing with the same problem, but disregarding the presence of adhesive layer, has shown that $N(0)$ is virtually independent of α when $\alpha > 3$. Therefore, the value $\alpha = 4$ is used exclusively in the numerical examples presented herein and the dependence of κ on α is suppressed anticipating that the conclusions reached hold for any value of α larger than 3.

The linear dependence of κ on $\lambda \geq 0.5$ was observed in [2] for the particular case of $\beta = E_2/E_1 = 1$. The same linear dependence of κ was numerically confirmed for a specific case $\epsilon = 0.01$ and $\beta = 20$. Based on these observations and Saint Venant's principle, we assume that

$$\kappa(\alpha, \lambda, \epsilon, \beta) = A(\epsilon, \beta) + B(\epsilon, \beta)\lambda \qquad (\alpha \geq 3, \lambda \geq 0.5, \epsilon > 0, \beta \geq 1). \tag{20}$$

The dependence of A and B on parameters ϵ and β is determined numerically and presented in Fig. 5. The solid curves show the variations of A and B upon β for a fixed value of $\epsilon = 0.01$. Alternatively, the dashed curves in Fig. 5 show the dependence of A and B upon ϵ^{-1} for a fixed value of $\beta = E_2/E_1 = 20$. The figure indicates that the effect of moduli ratio $\beta = E_2/E_1$ upon A and B is more pronounced than that of the thickness ratio $\epsilon = h_1/h$.

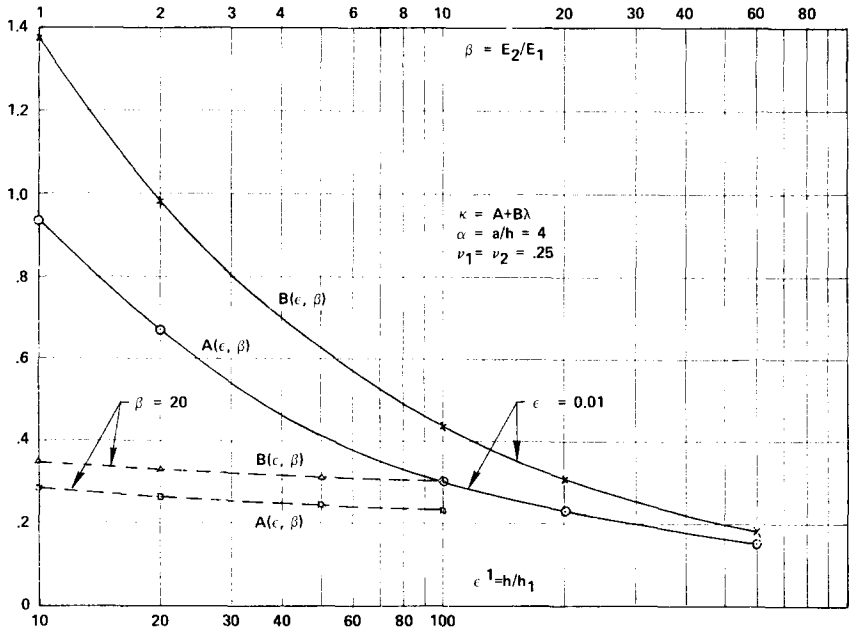

Fig. 5. Variation of functions A and B with ϵ and β.

Figure 6 presents the normalized intensity factor as a function of β and ϵ for $\lambda = 1, 2$. In this figure the solid lines are for a fixed thickness ratio $\epsilon = 0.01$ while β varies. The dashed curves in Fig. 6 are for a fixed moduli ratio $\beta = 20$ (aluminum-epoxy) while ϵ varies. Overall behavior of the curves in Fig. 6 is similar to that in Fig. 5. In particular, the dimensionless stress intensity factor decreases slightly as the thickness of adhesive layer decreases (β fixed). If we recall that a decrease in the stress intensity factor is equivalent to an increase of the rupture strength of the joint, the conclusion reached here supports the experimental observations by Bryand and Dukes[5] which indicate a slight decrease in joint strength with increasing adhesive thickness. This is also in agreement with the rule established by many observations and experiments that "a joint is stronger the thinner the adhesive layer in it". Figure 6 also shows that the rate of decrease in stress intensity factor (for a fixed combination of adherend and adhesive materials) due to a

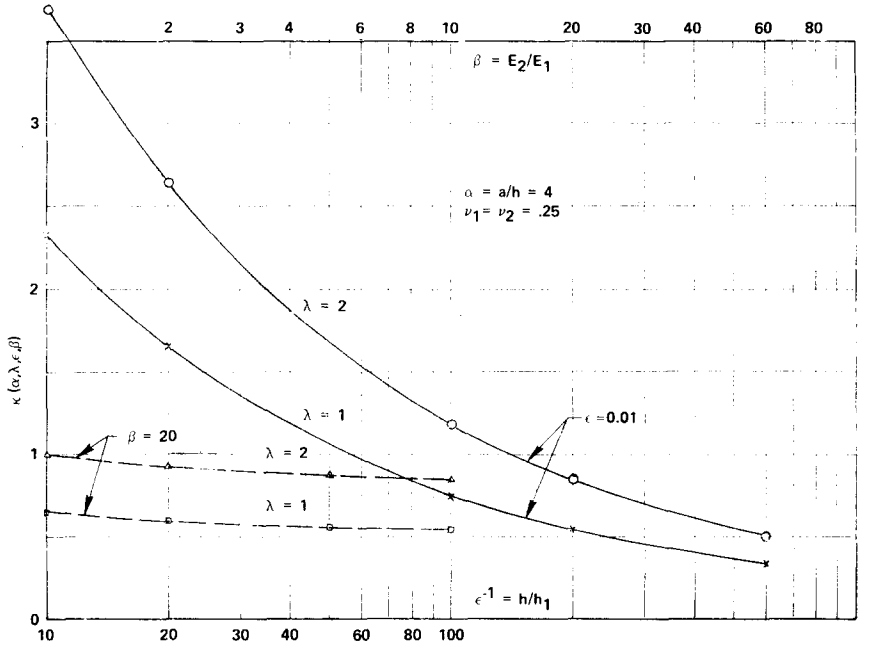

Fig. 6. Variation of stress intensity factor with β and ϵ.

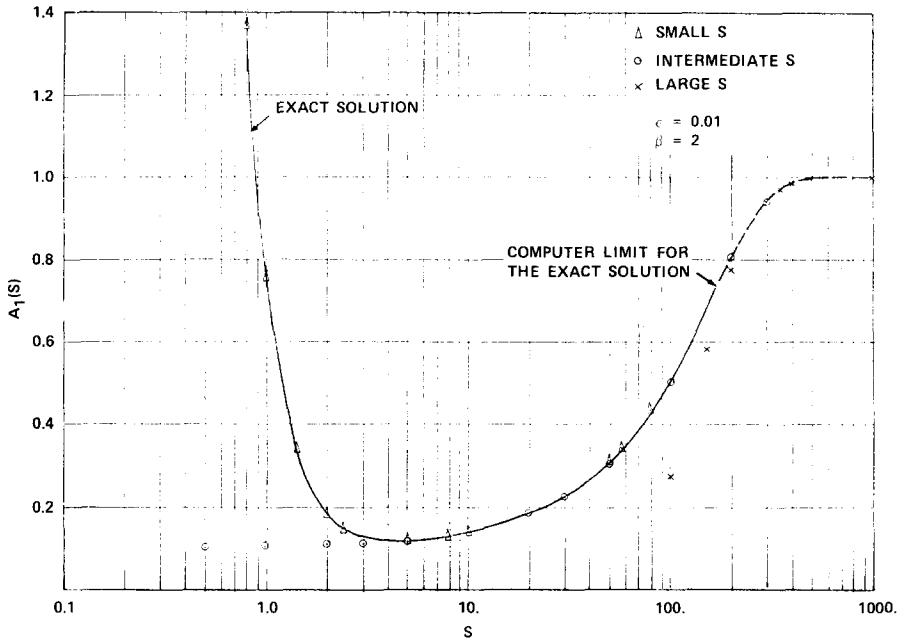

Fig. 7. Variation of A_1 with S.

decrease of adhesive thickness is small for the entire ϵ range considered ($10 \leq \epsilon^{-1} = h/h_1 \leq 100$). In particular the intensity factor remains almost constant for $h/h_1 > 60$.

In this numerical work, Poisson's ratios for the adherend and adhesive are assumed to be the same and the dependence of stress intensity factor upon Young's moduli and geometrical parameters is studied. If the stress intensity factor for an adhesive joint with a fixed geometrical configuration is desired for all possible material combinations, the most convenient presentation would be in terms of points in the α_*, β_* plane, [3, 6], since physically permissible combinations of material constants lie in a finite region in this plane.

4. CONCLUDING REMARKS

It would be anticipated by the chemist that the adhesive joint strength increases as the bond thickness decreases. The reason advanced is that the chemical bonding process (assuming clean

surfaces) results in a boundary layer of material along the adherend-adhesive interface that is stronger than that of either parent material. As the bond thickness decreases, a greater percentage of the adhesive is made up of this "stronger" material and hence a higher strength connection results.

The numerical results presented in the preceding section show that there is an alternative explanation for this behavior. The dependence of the mechanical stress field upon the bond line thickness is such that the connection strength must increase as the bond line thickness decreases and this fact should be included with the surface chemistry argument.

The strain energy release rate, $\mathcal{G}_I$, of the adhesive material in plane strain is related to the stress intensity factor by

$$\mathcal{G}_I = \frac{(1-\nu_1^2)}{E_1} K_I^2 \tag{21}$$

where ν_1, E_1 are the material properties of the adhesive. It is possible to measure[1] the critical value of $\mathcal{G}_I$ required to propagate a crack through the adhesive. Such experiments must necessarily be conducted on specific adherend-adhesive systems and as such only give strength values for the tested systems.

If one assumes that the basic material properties of the adhesive are independent of adherend and adhesive thickness, then the results presented herein can be used to determine the true adhesive strength, independent of the adherend-adhesive system used to measure it. Assuming the test configuration is one that can be modeled by the geometry used herein, then knowledge of the failure load permits the immediate evaluation of the critical value of K_I required to grow the crack. As the joint geometry and moduli ratio have been properly accounted for in the analysis, the resulting strength value of the adhesive is independent of these factors.

Acknowledgement—This work was supported by the National Science Foundation under Grant GK 30773 and ENG 74-18641.

REFERENCES

1. E. J. Ripling, S. Mostovoy and R. L. Patrick, Measuring fracture toughness of adhesive joints. *Material Research Standards* **4**(3), 139 (1964).
2. D. J. Chang, R. Muki and R. A. Westmann, Double cantilever beam models in adhesive mechanics. *Int. J. Solids Structures* **12**, 13 (1976).
3. J. Dundurs, Discussion on [4], *J. Appl. Mech.* **36**, 650 (1969).
4. D. Bogy, Edge-bonded dissimilar orthogonal elastic wedges under normal and shear loading. *J. Appl. Mech.* **35**, 460 (1968).
5. R. W. Bryant and W. A. Duke, The effect of adhesive thickness on joint strength. *J. Adhesion* **1**, 48 (1969).
6. D. Bogy, Two edge-bonded elastic wedges of different materials and wedge angles under surface tractions. *J. Appl. Mech.* **38**, 377 (1971).
7. J. J. Bikerman, *The Science of Adhesive Joints*, 2nd Edn. Academic Press, New York (1968).
8. J. D. Cole, *Perturbation Methods in Applied Mathematics*. Blaisdell, Waltam, Mass. (1968).

APPENDIX

In this appendix, the three alternative expressions of $A_1(s)$ suitable for numerical evaluation for large, intermediate and small values of s will be presented together with a brief explanation of their derivation. The function $A_1(s)$ is needed to evaluate $\hat{u}_{2,1}(x_1, 0)$ and, in turn, to solve the Fredholm integral equation for the normalized bond stress.

Exponential Fourier transform of Airy stress functions for $\hat{\tau}_{\alpha\beta}^{(1)}$ and $\hat{\tau}_{\alpha\beta}^{(2)}$ that satisfy the boundary conditions assume the following forms:

$$\begin{aligned}\hat{\psi}^{(1)}(z, x_2) &= \frac{1}{\sqrt{2\pi}z^2}\{\cosh(zx_2) + A_1(hz)[zx_2\cosh(zx_2) - \sinh(zx_2)] \\ &\quad + B_1(hz)zx_2\sinh(zx_2)\} \quad (0 < x_2 < h_1), \\ \hat{\psi}^{(2)}(z, x_2) &= \frac{1}{\sqrt{2\pi}z^2}\{A_2(hz)[z(x_2-h)\cosh(z(x_2-h)) - \sinh(z(x_2-h))] \\ &\quad + B_2(hz)z(x_2-h)\sinh(z(x_2-h))\} \quad (h_1 < x_2 < h),\end{aligned} \tag{A1}$$

where z is the transform parameter.

The continuity conditions for displacements and tractions along the line $x_2 = h_1$ lead to a system of four linear algebraic equations for A_1, A_2, B_1 and B_2. In the following derivation of the expressions of $A_1(s)$ we utilize the fact that the parameter $\epsilon = h_1/h$ is very small compared to unity.

Small values of s $(0 < s \leq 0.1\epsilon)$

We expand A_γ, B_γ $(\gamma = 1, 2)$ into power series of ϵ, substitute these into the simultaneous equations and equate terms of

equal power of ϵ. In this manner we arrive at

$$A_1(s) = \frac{k}{\sinh^2 s - s^2} \cdot \left[s + \frac{1}{2} \sinh(2s) \right] - 2\epsilon s \left[\bar{\omega} \cdot \left(f(s) + \frac{s^2}{\sinh^2(hs) - s^2} \right) + \frac{k \sinh^2(hs)}{\sinh^2 s - s^2} f(s) \right] + 0\left(\frac{\epsilon^2}{s^3}\right) \quad \text{as } s \to 0, \epsilon \to 0 \tag{A2}$$

where k is given by (11) and

$$f(s) = \bar{\omega} + \frac{(k-1)\sinh^2 s}{\sinh^2 s - s^2}, \tag{A3}$$

$$\bar{\omega} = \frac{\alpha_* - \beta_*}{\alpha_* - 1}.$$

Large values of s $(4\epsilon^{-1} < s < \infty)$

Recall first that a neighborhood of the point at infinity in the transformed domain (s-plane) corresponds to the neighborhood of the origin in the physical x_1x_2-plane. We therefore consider a problem of an infinite slab bonded to a half plane. This assembly is subjected to the boundary and regularity conditions:

$$\left.\begin{aligned} \hat{\tau}_{22}^{(1)}(x_1, 0) = -\delta(x_1), \quad \hat{\tau}_{12}^{(1)}(x_1, 0) = 0 \quad (-\infty < x_1 < \infty), \\ \hat{\tau}_{\alpha\beta}^{(\gamma)} = o(1) \quad (\gamma = 1, 2) \quad \text{as } x_\alpha x_\alpha \to \infty. \end{aligned}\right\} \tag{A4}$$

Note that the transform of the stress functions for the slab is still given by the first of (A1) and that for the half plane has a simple form. After routine manipulation, one is led to

$$\begin{aligned} A_1(s) &= \frac{q_1 - 4\epsilon s\, e^{-2\epsilon s} + q_2 e^{-4\epsilon s}}{q_1 + [1 - q_1 q_2 + 4(\epsilon s)^2] e^{-2\epsilon s} - q_2 e^{-4\epsilon s}} \\ &= 1 - [1 - q_1 q_2 + 4\epsilon s + 4(\epsilon s)^2] \frac{e^{-2\epsilon s}}{q_1} + 0((\epsilon s)^4 e^{-4\epsilon s}) \quad \text{as} \quad s \to \infty, \epsilon \to 0 \end{aligned} \tag{A5}$$

where

$$q_1 = \frac{\beta_* - 1}{\alpha_* - \beta_*}, \quad q_2 = \frac{\alpha_* + \beta_*}{\beta_* + 1}. \tag{A6}$$

Intermediate values of s $(0.1\epsilon^{-1} < s < 4\epsilon^{-1})$

Representation of $A_1(s)$ suitable for evaluation in this interval is obtained by use of two variable expansion procedures [8]. The system of linear algebraic equations for A_1, A_2, B_1, B_2 is rewritten in terms of the large variable s, a small variable $\bar{s} = \epsilon s$ and the small parameter ϵ. These equations together with the two approximate representations of A_1, A_2, B_1, B_2 for small and large values of s (those for A_2, B_1, B_2 are not presented here since they are not needed in the subsequent analysis) suggest the expressions:

$$\begin{aligned} A_1(s) &= a_{11}(\bar{s}) + 0(\epsilon), \\ B_1(s) &= b_{11}(\bar{s}) + 0(\epsilon), \\ A_2(s) &= \sum_{i=1}^{N} a_{2i}(\bar{s}) \bar{a}_i(s) + 0(\epsilon), \\ B_2(s) &= \sum_{i=1}^{N} b_{2i}(\bar{s}) \bar{b}_i(s) + 0(\epsilon). \end{aligned} \tag{A7}$$

Substitution of A_1, B_1, A_2, B_2 from (A7) into the system of linear algebraic equations and subsequently equating the terms of equal power of ϵ yields

$$\begin{aligned} A_1(s) = \{&[(1-\bar{\omega})(2k+\bar{\omega}) + \bar{\omega}] \sinh(2\bar{s}) + 2k \cosh(2\bar{s}) - 2\bar{\omega}(2k+\bar{\omega})\bar{s}\} / \{2k \sinh(2\bar{s}) \\ &+ [(1-\bar{\omega})(2k+\bar{\omega}) + \bar{\omega}] \cosh(2\bar{s}) + 2\bar{\omega}(2k+\bar{\omega})\bar{s}^2 + \bar{\omega}^2 + 2(k-1)(\bar{\omega}-1)\} + 0(\epsilon) \end{aligned} \tag{A8}$$

where k and $\bar{\omega}$ are given by (11) and (A3), respectively.

In Fig. 7 the solid curve represents $A_1(s)$ obtained by solving the original system of linear equations numerically while the triangles, circles, and crosses are, in this order, the values evaluated from (A2), (A7) and (A5), respectively. The dashed curve represents the portion of A_1 where some of the functions involved become too large for the computer to handle. The percentage errors of approximate expressions in (A2), (A5) and (A7) were confirmed to be less than 0.1% for all the examples treated numerically in this paper.